

In-Plane Mechanical Characterization of a Kevlar[®] Composite

Rene Alejandro Cancoco de la Cruz¹, Caleb Carreño Gallardo¹, Alberto Diaz Diaz¹,
Luis Adrian Zuñiga Aviles², Gabriel Plascencia Barrera¹ and Jose Martin Herrera Ramirez^{1,*}

¹ Centro de Investigación en Materiales Avanzados, S.C. (CIMAV), Av. Miguel de Cervantes #120, Complejo Industrial Chihuahua, Chihuahua 31136, Mexico; rene.canceco@cimav.edu.mx (R.A.C.d.I.C.); caleb.carreno@cimav.edu.mx (C.C.G.); alberto.diaz@cimav.edu.mx (A.D.D.); gabriel.plascencia@cimav.edu.mx (G.P.B.)

² Facultad de Medicina, Universidad Autonoma del Estado de México, Toluca 50180, Mexico; adriandgim@gmail.com

* Correspondence: martin.herrera@cimav.edu.mx

Abstract: Polymer-based composites are widely used in the automotive, security, aeronautical and space industries, to mention a few. This is because of their good mechanical properties, which are similar to those of metals but with the attraction of being lightweight. Kevlar[®] is extensively used as a reinforcement in the security industry owing to its good ballistic properties. This investigation presents a mechanical characterization based on in-plane quasi-static tensile testing of Kevlar[®] 29/phenolic resin with a polyvinyl butyral composite using a universal testing system. The methodology developed for the preparation of the coupons is based on pressure, temperature and time. As a result of this work, elastic moduli (E_L and E_T), Poisson's ratio (ν_{LT}), shear modulus (G_{LT}) and strengths (X_T , Y_T , S) were obtained. It is worth mentioning that there is scarce or no characterization of this material in the literature, and those studies that do characterize it do not present the coupons' thermoforming conditions or the reasons for the coupons' dimensions (width, length and thickness).

Keywords: Kevlar[®]; polymer composite; mechanical properties; quasi-static tensile test



Citation: Cancoco de la Cruz, R.A.; Carreño Gallardo, C.; Diaz Diaz, A.; Zuñiga Aviles, L.A.; Plascencia Barrera, G.; Herrera Ramirez, J.M. In-Plane Mechanical Characterization of a Kevlar[®] Composite. *Fibers* **2024**, *12*, 38. <https://doi.org/10.3390/fib12050038>

Academic Editors: Deesy Gomes Pinto, Ana Martins Amaro and Luis Filipe Almeida Bernardo

Received: 23 February 2024

Revised: 4 April 2024

Accepted: 19 April 2024

Published: 25 April 2024



Copyright: © 2024 by the authors. Licensee MDPI, Basel, Switzerland. This article is an open access article distributed under the terms and conditions of the Creative Commons Attribution (CC BY) license (<https://creativecommons.org/licenses/by/4.0/>).

1. Introduction

Fiber-reinforced composites are now firmly at the forefront of advanced materials and are used in an increasing number of applications, from fishing rods to satellites. Today, the largest use of high-performance composites is in civilian applications, but initially they were mainly used in the military and, in particular, in aerospace structures. The reason for the use of these materials is due to weight savings [1].

The present work consisted of the in-plane characterization of a Kevlar[®] material preimpregnated with phenolic resin with polyvinyl butyral on both sides. As the first stage of this study, our aim was to determine the mechanical properties of the in-plane interweaving through tensile tests based on a standard method using a universal testing system to acquire the elastic moduli and strengths. The elastic constants obtained from this study will be used for a subsequent improvement study of an antifragment helmet using the finite element method. In the literature, there are studies that can be classified according to the geometry under study, either focused on military helmets or on rectangular geometries subjected to a ballistic impact using computational tools such as LS-DYNA[®] or ABAQUS[®] (Table 1). The mechanical properties used in this type of research come from the study carried out by van Hoof et al. in 2001 [2,3], who was a pioneer of the use of numerical simulations of ballistic impact on reinforcement laminates of Kevlar[®] 29/phenolic material. Hoof [2] simulated a rectangular-geometry piece of laminate that was impacted by a projectile fragment; in his numerical simulation he took the mechanical properties of Kevlar[®] from Guoqi et al. [4], who in turn characterized the Kevlar[®] 29/polyester material through quasi-static and dynamic tests in 1981 [4]. From the validation, van Hoof observed

that there was no correlation between the numerical simulation and the ballistic test, therefore a “calibration” of the mechanical properties (strengths) was carried out to force a correlation. From this work, the parameters of the Kevlar[®] material were obtained, which are still used today for ballistic studies on combat helmets [5–12], as shown in Table 1.

Table 1. In-plane mechanical properties of Kevlar[®] found in the literature.

Mechanical Property	Rectangular Plate				Helmet		
	Kevlar 29/Phenolic	Kevlar 29/Epoxy	Kevlar 29/Epoxy	Kevlar 29/Epoxy	Kevlar	Kevlar 29	Kevlar
E_L [GPa], Longitudinal elastic modulus	18.5	18.5	7.618	10.06	18	18.5	18.5
E_T [GPa], Transversal elastic modulus	18.5	18.5	11.05	10.06	18	18.5	18.5
ν_{LT} , Poisson’s ratio L-T	0.25	0.25	0.18	0.25	0.25	0.25	0.25
G_{LT} [GPa], Shear modulus in L-T plane	0.77	0.77	2.123	0.77	0.77	0.77	0.77
X_T [MPa], Tensile strength in longitudinal direction	555 ⁽²⁾	1850 ⁽¹⁾	400	425	555	555	555
Y_T [MPa], Tensile strength in transversal direction	555 ⁽²⁾	1850 ⁽¹⁾	530	425	555	555	555
S [MPa], Shear strength in L-T direction	77	77	67	77	77	77	77
Autor	van Hoof [2]	Bresciani et al. [11]	Nunes et al. [13]	Scazzosi et al. [14]	Tan et al. [9]	Caçoilo et al. [8]	Lee and Gong [6]

⁽¹⁾ Strength property adopted “initially” in the numerical model for woven Kevlar[®] by van Hoof [2]. ⁽²⁾ Strength property adopted “finally” in the numerical model for woven Kevlar[®] by van Hoof et al. [2,3].

The methodology used by Guoqi et al. [4] to obtain the elastic moduli in the warp and weft directions was through the use of coupons with interleaved layers at $[0^\circ, 90^\circ]$, obtaining an elastic modulus of 18.5 GPa for both orthotropy directions; therefore, no distinction was made between the principal directions of the material. In addition, the way in which the shear modulus was characterized is not recommended, since it generates undesirable deformations at the ends of the coupons. Therefore, our work proposes a methodology based on symmetrical laminates with straight coupons at $[+45^\circ, -45^\circ]_s$ that can be used to obtain the shear modulus G_{LT} to prevent the coupons from generating moments in the universal testing system grips.

In the research presented by Nunes et al. [13], a Kevlar[®] 29/epoxy composite was intensively characterized in the plane through tensile, compression, V-notch rail shear and short beam tests. Also, Scazzosi et al. [14] determined the mechanical properties of a Kevlar[®] 29/epoxy composite in the plane by tensile tests. In the research by Gower et al. [15], Kevlar[®] 129 was characterized through a tensile test, but neither the thermoforming conditions nor the coupon’s dimensions were exposed.

Shim et al. [16] analyzed the Twaron CT 716 through dynamic tests using a Hopkinson tension bar machine to study the viscoelasticity effect; the tests were performed at strain rates of 280–550 s^{-1} . Quasi-static tests were also performed with a universal testing system at strain rates from 10^{-3} to $1 s^{-1}$. At high strain rates, the material behaves more rigidly, but it fails at very small strains. While this work is ideal for the study of dynamically loaded materials, not all laboratories have the necessary equipment, such as the Hopkinson tension bar.

There are a limited number of works in the literature that characterize a Kevlar[®] material embedded in thermosetting resin [17]. Even though Kevlar[®] 29/phenolic resin with polyvinyl butyral is not a novel material [2,3,18], the intention of our work is to

provide a methodology to characterize the material in the plane using quasi-static tensile tests in each of the orthotropic directions of the Kevlar® composite. Subsequently, the goal is to characterize the material in terms of its thickness and build a finite element model of an antifracture helmet considering different orientations of the layers within the laminate in order to protect against the impact of a fragment simulating a projectile. Finally, the model will be validated with an impact test. For all of this, it is necessary to be certain of the mechanical properties of the material under study to avoid discrepancies between the numerical simulation and the experimental validation.

A woven fabric can be studied as an orthotropic material with nine elastic constants represented in a matrix of compliances, as shown in Equation (1) [19]. The matrix considers the elastic moduli (E_L, E_T, E_N), shear moduli (G_{LT}, G_{TN}, G_{LN}) and Poisson’s ratio ($\nu_{TL}, \nu_{NL}, \nu_{NT}$). The subscripts L, T and N represent the orthotropic directions of a woven fabric as shown in Figure 1. The aim of this work is to characterize the Kevlar® material in the L-T plane.

$$\begin{pmatrix} \varepsilon_L \\ \varepsilon_T \\ \varepsilon_N \\ 2\varepsilon_{TN} \\ 2\varepsilon_{LN} \\ 2\varepsilon_{LT} \end{pmatrix} = \begin{bmatrix} \frac{1}{E_L} & -\frac{\nu_{TL}}{E_T} & -\frac{\nu_{NL}}{E_N} & 0 & 0 & 0 \\ -\frac{\nu_{LT}}{E_L} & \frac{1}{E_T} & -\frac{\nu_{NT}}{E_N} & 0 & 0 & 0 \\ -\frac{\nu_{LN}}{E_L} & -\frac{\nu_{TN}}{E_T} & \frac{1}{E_N} & 0 & 0 & 0 \\ 0 & 0 & 0 & \frac{1}{G_{TN}} & 0 & 0 \\ 0 & 0 & 0 & 0 & \frac{1}{G_{LN}} & 0 \\ 0 & 0 & 0 & 0 & 0 & \frac{1}{G_{LT}} \end{bmatrix} \begin{pmatrix} \sigma_L \\ \sigma_T \\ \sigma_N \\ \sigma_{TN} \\ \sigma_{LN} \\ \sigma_{LT} \end{pmatrix} \tag{1}$$

In brief: $\varepsilon = c \cdot \sigma$, where ε represents the vector of strains, C is the matrix of the compliances in the orthotropic direction and σ is the vector of stresses. According to symmetry: $\nu_{TL} = \nu_{LT} \frac{E_T}{E_L}$, $\nu_{NL} = \nu_{LN} \frac{E_N}{E_L}$, $\nu_{NT} = \nu_{TN} \frac{E_T}{E_N}$. The principal material directions of the individual layers within the laminate will not necessarily coincide with the global laminate axis. The stiffness R' and compliance C' matrix for each layer must be expressed within the global material axis of the laminate using the following transformations given in Equations (2) and (3).

$$R' = O_\sigma \cdot R \cdot O_\sigma^{-1} = O_\sigma \cdot R \cdot O_\sigma^t \tag{2}$$

$$C' = O_\varepsilon \cdot C \cdot O_\varepsilon^{-1} = O_\varepsilon \cdot C \cdot O_\varepsilon^t \tag{3}$$

where O_σ and O_ε represent the rotation matrices used to obtain the compliance matrix in the global axis system, according to Equation (4) and Equation (5), respectively.

$$O_\sigma = \begin{pmatrix} c^2 & s^2 & 0 & 0 & 0 & -2cs \\ s^2 & c^2 & 0 & 0 & 0 & 2cs \\ 0 & 0 & 1 & 0 & 0 & 0 \\ 0 & 0 & 0 & c & s & 0 \\ 0 & 0 & 0 & -s & c & 0 \\ cs & -cs & 0 & 0 & 0 & c^2 - s^2 \end{pmatrix} \tag{4}$$

$$O_\varepsilon = \begin{pmatrix} c^2 & s^2 & 0 & 0 & 0 & -cs \\ s^2 & c^2 & 0 & 0 & 0 & cs \\ 0 & 0 & 1 & 0 & 0 & 0 \\ 0 & 0 & 0 & c & s & 0 \\ 0 & 0 & 0 & -s & c & 0 \\ 2cs & -2cs & 0 & 0 & 0 & c^2 - s^2 \end{pmatrix} \tag{5}$$

where $c = \cos \theta$ and $s = \sin \theta$. Finally, the vectors of stresses σ' and strains ε' in the global axis system are determined by Equation (6) and Equations (7), respectively.

$$\sigma' = R' \cdot \varepsilon' \tag{6}$$

$$\varepsilon' = C' \cdot \sigma' \tag{7}$$

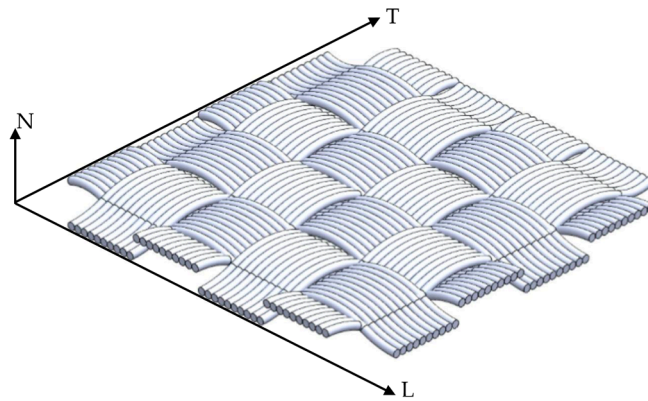


Figure 1. Orthotropic directions of a woven material: longitudinal (L), transversal (T) and normal to the L - T plane (N).

For a plane stresses study, Equation (1) becomes Equation (8). In the first stage of this work, the composite material was characterized in the plane using tensile tests. The matrix of compliances in Equation (8) is required to determine the elastic moduli (E_L and E_T), shear modulus (G_{LT}), Poisson's ratio (ν_{TL}) and strengths (X_T , Y_T and S).

$$\begin{Bmatrix} \varepsilon_L \\ \varepsilon_T \\ 2\varepsilon_{LT} \end{Bmatrix} = \begin{bmatrix} \frac{1}{E_L} & -\frac{\nu_{TL}}{E_T} & 0 \\ -\frac{\nu_{LT}}{E_L} & \frac{1}{E_T} & 0 \\ 0 & 0 & \frac{1}{G_{LT}} \end{bmatrix} \begin{Bmatrix} \sigma_L \\ \sigma_T \\ \sigma_{LT} \end{Bmatrix} \quad (8)$$

2. Materials and Methods

Figure 2a shows one sheet of Kevlar[®] 29/phenolic resin with polyvinyl butyral used for the production of antifragement helmets. This material is preimpregnated with resin on both sides. As shown in the image, the material has horizontal and vertical cuts, as it has been prepared for use in the manufacture of helmets; these cuts limited the extraction of the coupons. For the development of this in-plane testing program, straight geometries based on the ASTM D3039/D3039M standard [20] were implemented to determine elastic moduli (E_L , E_T), shear modulus (G_{LT}), Poisson's ratio (ν_{LT}) and strengths (X_T , Y_T , S) through tensile tests. Straight coupons are beneficial when a water-jet cutting machine is not available, facilitating the cutting process of each layer by using sheet-metal-cutting scissors. A Hitachi[®] scanning electron microscope model SU3500 was used to identify the orthotropic directions (Figure 2b); a repetitive unit size of 3 mm was observed, with the yarn width being greater in the longitudinal direction than in the transversal direction. The orthotropic directions of each sheet were identified in order to produce coupons with the properly identified directions.

Figure 3 shows the coupon geometry, as well as the dimensions and number of locally thermoformed tabs at the coupons' ends, which were used to protect the material from the universal machine grips and ensure the coupon breakage occurred away from the grips. A coupon width of 32 mm was considered, taking into account that, to obtain the Poisson's ratio ν_{LT} , a strain gage has to be positioned transversely to the coupon. The material was cut according to the orthotropic directions, as shown in Figure 1. The coupon length used was 197 mm, which represents the maximum length that it was possible to obtain from the as-received material. For the tabs, it was proposed that we should make a smooth transition in the thickness of the coupons and thus avoid a pronounced concentration of stresses.

The grid length in the longitudinal direction of the gage is 12.7 mm, which is large enough to cover 4.2 repeat units of the woven fabric and thus to obtain a correct measurement of the Poisson's ratio ν_{TL} . During the tensile test, large strains were expected, so EP-08-500GB-120 gages (Micro-Measurements, Raleigh, NC, USA) were selected, which can be used for applications of up to $\pm 20\%$; these gages have a resistance of 120 Ω , which the equipment can read.

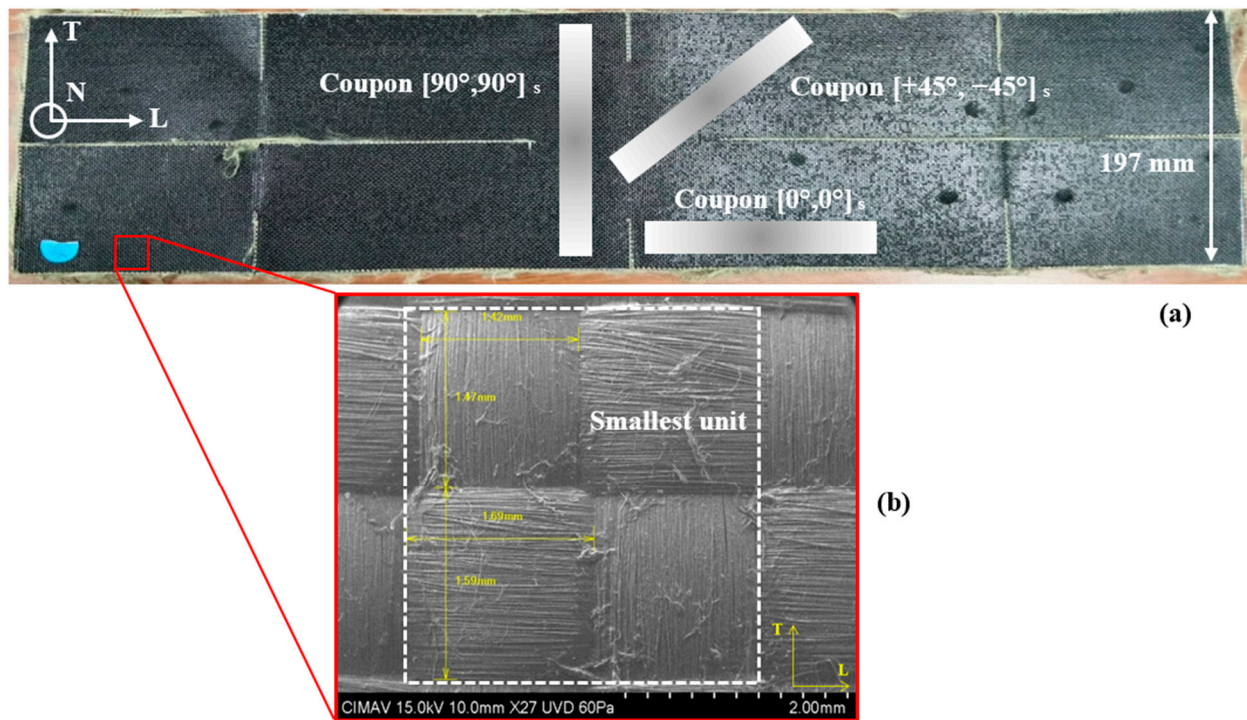


Figure 2. (a) As-received Kevlar[®] 29/phenolic resin with polyvinyl butyral material indicating where the coupons were taken from. (b) Scanning electron microscopy image for the identification of the orthotropic directions.

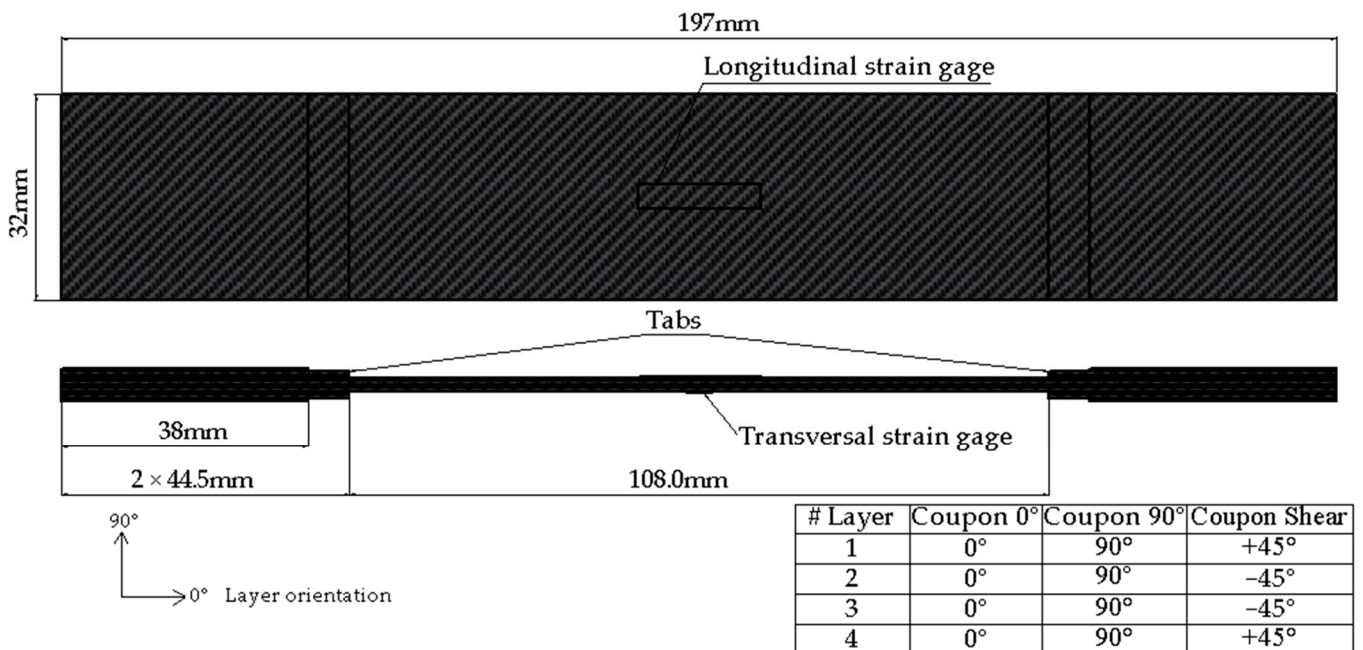


Figure 3. Geometry of coupons for the in-plane characterization.

A mold and cover were designed and fabricated from 6.35 cm × 25.4 cm × 1.27 cm AISI 1018 steel plates. The thickness of 1.27 cm was chosen to avoid buckling in the middle of the plate during the manufacturing of the mold. Figure 4a shows the stacking of resin-impregnated Kevlar[®] layers; the use of Teflon[®] paper was necessary to prevent the sample from sticking to the mold. Figure 4b shows the closed mold and Figure 4c shows a Carver[®] 4122 Manual Heated Press (10 t) where the coupon thermoforming process was performed. The thermoforming conditions were 192 °C with a compression load of 6.5 t for

10.5 min, which were based on the manufacturing conditions of the antifragement helmets. The compression load and time conditions applied to the tabs were reduced to 2 t and 3 min, respectively, to avoid a local reduction in the thickness of the coupons' ends.

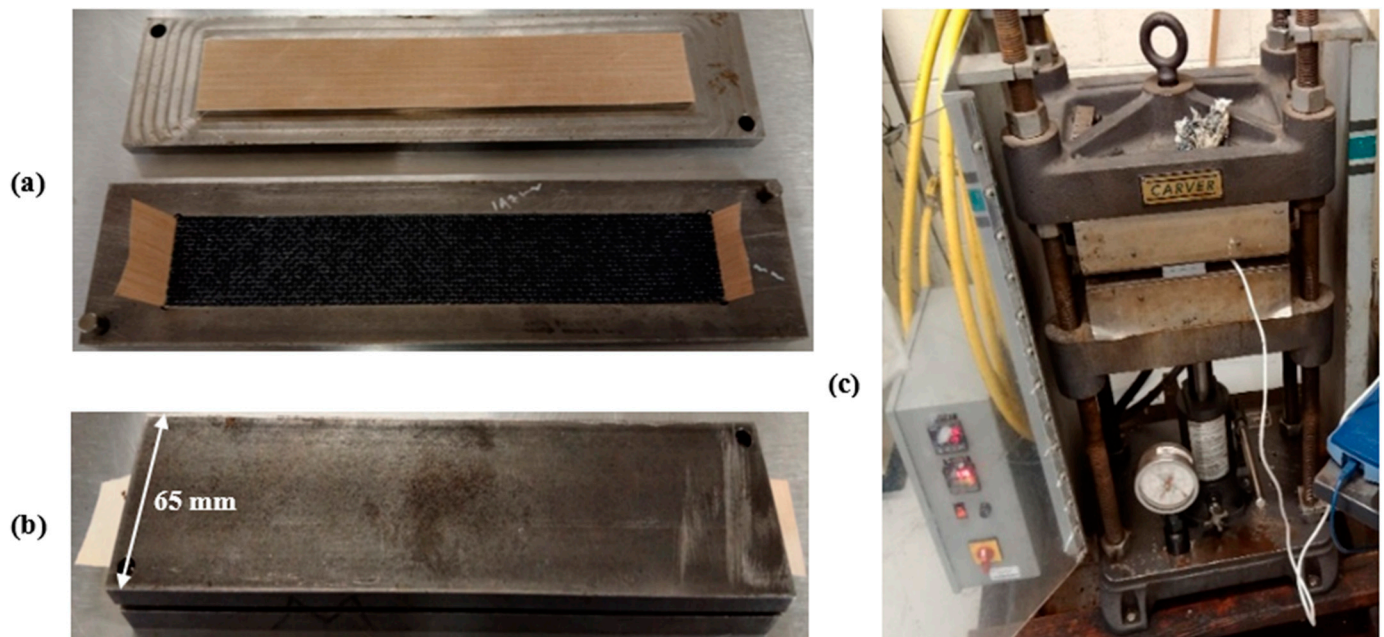


Figure 4. (a) Stacking of layers in the mold. (b) Closing the mold prior to thermoforming of coupon. (c) Carver® 4122 Manual Heated Press.

For the tensile test, an Instron® 3382 universal testing system was used (Figure 5). A head displacement rate of 2 mm/min (0.019 min^{-1}) was used, according to the ASTM D3039/D3039M standard [20]. Mechanical wedge-action grips type 2716-003 were used.



Figure 5. Tensile test performed on a coupon instrumented with strain gages using an Instron® 3382 universal testing system (Instron, Norwood, MA, USA).

Jones [21] proposed determining the shear modulus G_{LT} using a tensile test instead of using the Iosipescu method, which requires special grips that are not available in most laboratories. To perform this test, the layers are required to be oriented at 45° and, using Equation (9), it is possible to determine the shear modulus in the G_{LT} plane; E_x is the elastic modulus with the material oriented at 45° . Jones' method generates angular strains at the end of the coupon's edges when the ends of the laminate are free to deform, as shown on the left side of Figure 6. However, if the ends of the coupon are clamped, this causes the coupon to twist and generate moments at gripping points, as shown on the right side of Figure 6.

$$G_{LT} = \left(\frac{1}{\frac{4}{E_x} - \frac{1}{E_L} + \frac{2\nu_{LT}}{E_L} - \frac{1}{E_T}} \right) \tag{9}$$

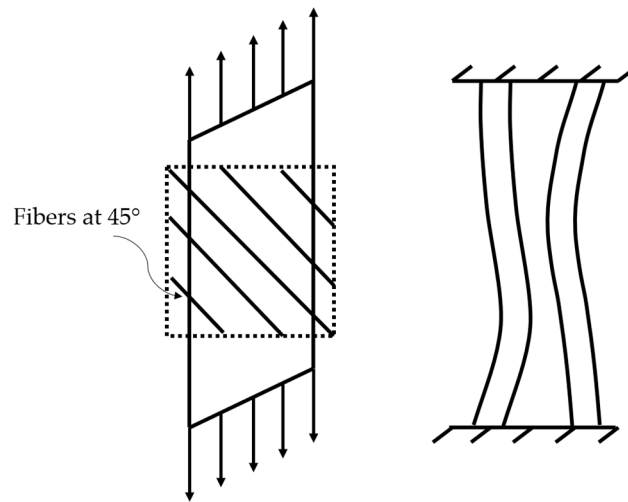


Figure 6. Deformation of a unidirectional reinforced laminate loaded at 45° to the fibers (adapted from [21]).

An alternative procedure to the Jones' equation is presented below, which can be used to obtain the shear modulus G_{LT} using straight coupons at $[+45^\circ, -45^\circ]_s$ by performing tensile tests using a universal testing system, as shown in Figure 3. This methodology avoids deformations such as those shown in Figure 6.

In the case of a laminate, the total force and moment resultants can be obtained by adding the effects of all layers in a single-layer element, as shown in Figure 7.

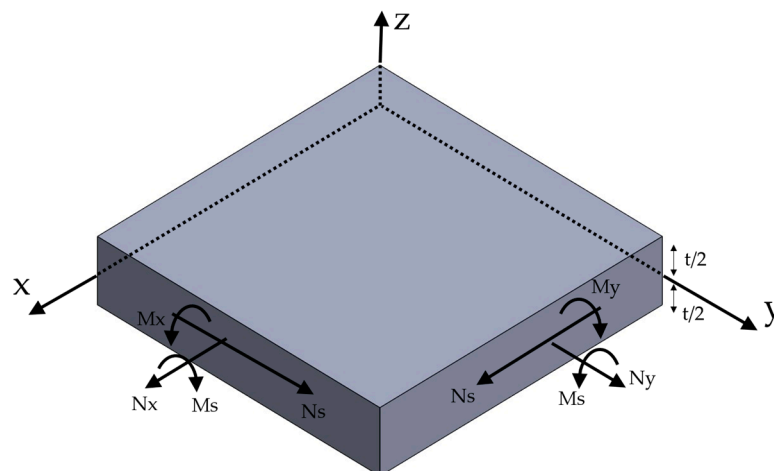


Figure 7. Element made of a single layer with resultant forces and moments (adapted from [16]).

The force–deformation relationship and the moment–deformation relationship are described by Equation (10) and Equation (11), respectively [19]:

$$\begin{bmatrix} N_x \\ N_y \\ N_s \end{bmatrix} = \begin{bmatrix} A_{xx} & A_{xy} & A_{xs} \\ A_{yx} & A_{yy} & A_{ys} \\ A_{sx} & A_{sy} & A_{ss} \end{bmatrix} \begin{bmatrix} \varepsilon_x \\ \varepsilon_y \\ \gamma_s \end{bmatrix} + \begin{bmatrix} B_{xx} & B_{xy} & B_{xs} \\ B_{yx} & B_{yy} & B_{ys} \\ B_{sx} & B_{sy} & B_{ss} \end{bmatrix} \begin{bmatrix} \kappa_x \\ \kappa_y \\ \kappa_s \end{bmatrix} \quad (10)$$

$$\begin{bmatrix} M_x \\ M_y \\ M_s \end{bmatrix} = \begin{bmatrix} B_{xx} & B_{xy} & B_{xs} \\ B_{yx} & B_{yy} & B_{ys} \\ B_{sx} & B_{sy} & B_{ss} \end{bmatrix} \begin{bmatrix} \varepsilon_x \\ \varepsilon_y \\ \gamma_s \end{bmatrix} + \begin{bmatrix} D_{xx} & D_{xy} & D_{xs} \\ D_{yx} & D_{yy} & D_{ys} \\ D_{sx} & D_{sy} & D_{ss} \end{bmatrix} \begin{bmatrix} \kappa_x \\ \kappa_y \\ \kappa_s \end{bmatrix} \quad (11)$$

where N_x, N_y are the normal forces per unit length, N_s is the shear force per unit length, M_x and M_y are the bending moments per unit length and M_s is the twisting moment per unit length [19].

Equations (10) and (11) can be combined into one general expression that briefly relates the in-plane forces and moments to the reference plane strains and curvatures, as indicated by Equation (12):

$$\begin{bmatrix} N \\ M \end{bmatrix} = \begin{bmatrix} A & B \\ B & D \end{bmatrix} \begin{bmatrix} \varepsilon^\circ \\ \kappa \end{bmatrix} \quad (12)$$

The above relationships are expressed in terms of three laminate stiffness matrices, $[A]$, $[B]$ and $[D]$, which are functions of the thickness, material properties and stacking sequence of the individual layers. $[A]$ is the extensional stiffness matrix expressed by Equation (13), which relates in-plane forces to in-plane strains; $[B]$ is the coupling stiffness matrix expressed by Equation (14), which relates in-plane forces to curvatures and moments to in-plane strains. $[D]$ is the bending laminate stiffness matrix expressed by Equation (15), which relates moments to curvatures [19].

$$A = \sum_{i=1}^n h_i (C_i')^{-1} \quad (13)$$

$$B = \sum_{i=1}^n e_i h_i (C_i')^{-1} \quad (14)$$

$$D = \sum_{i=1}^n \left[e_i (h_i)^2 + \frac{e_i^3}{12} \right] (C_i')^{-1} \quad (15)$$

where e_i represents the vector of thickness for each layer and C_i' is the matrix of compliances in the global system. As in symmetric laminates, $B = 0$; therefore, there is no coupling between in-plane loading and out-of-plane deformation (curvatures) and between bending and twisting moments and in-plane deformation. These laminates exhibit no distortion or warpage after fabrication and are easier to analyze. Therefore, Equation (10) and Equation (11) become Equation (16) and Equation (17), respectively:

$$\begin{bmatrix} N_x \\ N_y \\ N_s \end{bmatrix} = \begin{bmatrix} A_{xx} & A_{xy} & A_{xs} \\ A_{yx} & A_{yy} & A_{ys} \\ A_{sx} & A_{sy} & A_{ss} \end{bmatrix} \begin{bmatrix} \varepsilon_x \\ \varepsilon_y \\ \gamma_s \end{bmatrix} \quad (16)$$

$$\begin{bmatrix} M_x \\ M_y \\ M_s \end{bmatrix} = \begin{bmatrix} D_{xx} & D_{xy} & D_{xs} \\ D_{yx} & D_{yy} & D_{ys} \\ D_{sx} & D_{sy} & D_{ss} \end{bmatrix} \begin{bmatrix} \kappa_x \\ \kappa_y \\ \kappa_s \end{bmatrix} \quad (17)$$

When an axial load N_X is applied through a universal testing system to a coupon with a configuration of four layers $[+45^\circ, -45^\circ]_s$, according to Equation (16), $N_y = N_s = 0$ and

$\gamma_s = 0$ (the edges remain straight), and ϵ_x and ϵ_y are different of zero. Inverting matrix A from Equation (16) yields Equation (18) which can be used to obtain ϵ_x .

$$\epsilon_x = \frac{\{N_x [E_L^2 + E_L E_T + 4E_L G_{LT} + 2E_L E_T \nu_{LT} - 4E_T G_{LT} \nu_{LT}^2]\}}{[16E_L e (E_L G_{LT} + E_T G_{LT} + 2E_T G_{LT} \nu_{LT})]} \quad (18)$$

where e is the thickness of each layer considering/in this case/that each layer has the same thickness. $\sigma_x = \frac{N_x}{4e}$ represents the average stress across all of the layers because the stress changes from layer to layer and $E_{\mp 45_S} = \frac{\sigma_x}{\epsilon_x}$, thus obtaining the shear modulus G_{LT} (Equation (19)).

$$G_{LT} = \frac{E_{\mp 45_S} E_L (E_L + E_T + 2E_T \nu_{LT})}{4[E_L (E_L + E_T + 2E_T \nu_{LT}) + E_{\mp 45_S} (E_T \nu_{LT}^2 - E_L)]} \quad (19)$$

If $E_L = E_T$, Equation (19) becomes Equation (20).

$$G_{LT} = \frac{2E_{\mp 45_S} E_L (E_L + E_T \nu_{LT})}{4[2E_L (E_L + E_L \nu_{LT}) + E_{\mp 45_S} (E_L \nu_{LT}^2 - E_L)]} \quad (20)$$

3. Results and Discussion

Figure 8 shows the tensile stress–strain curves of four coupons tested at 0° (longitudinal direction). It is worth mentioning that three of them (EL-2, EL-3, EL-4) did not reach the strength or strain of coupon EL-1 due to the debonding of their tabs; however, the four coupons performed similarly in the 0–2% strain range, which was adequate to calculate the longitudinal elastic modulus ($E_L = 11.78 \pm 1.07$ GPa). Two additional coupons (EL-5, EL-6) with no strain gage instrumentation were tested to determine a suitable strength ($X_T = 648.33 \pm 56.31$ MPa) (Figure 9).

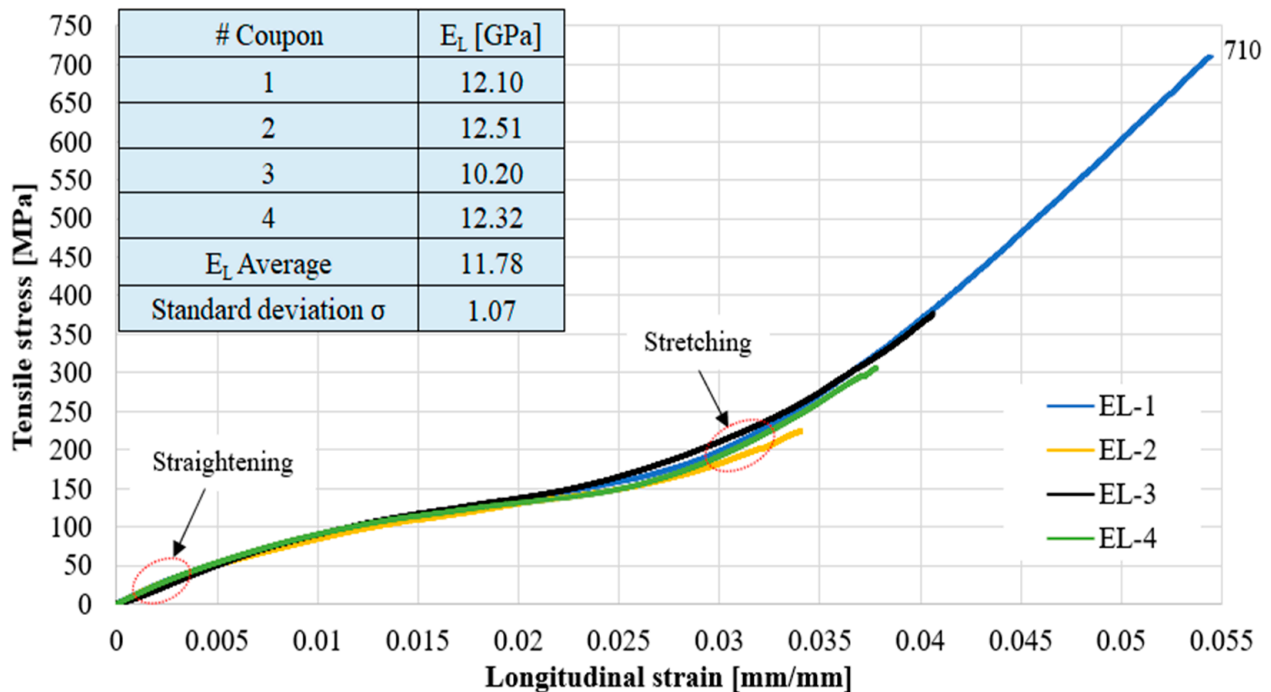


Figure 8. Tensile stress–strain curves of coupons tested at 0° . Strain measured with strain gages.

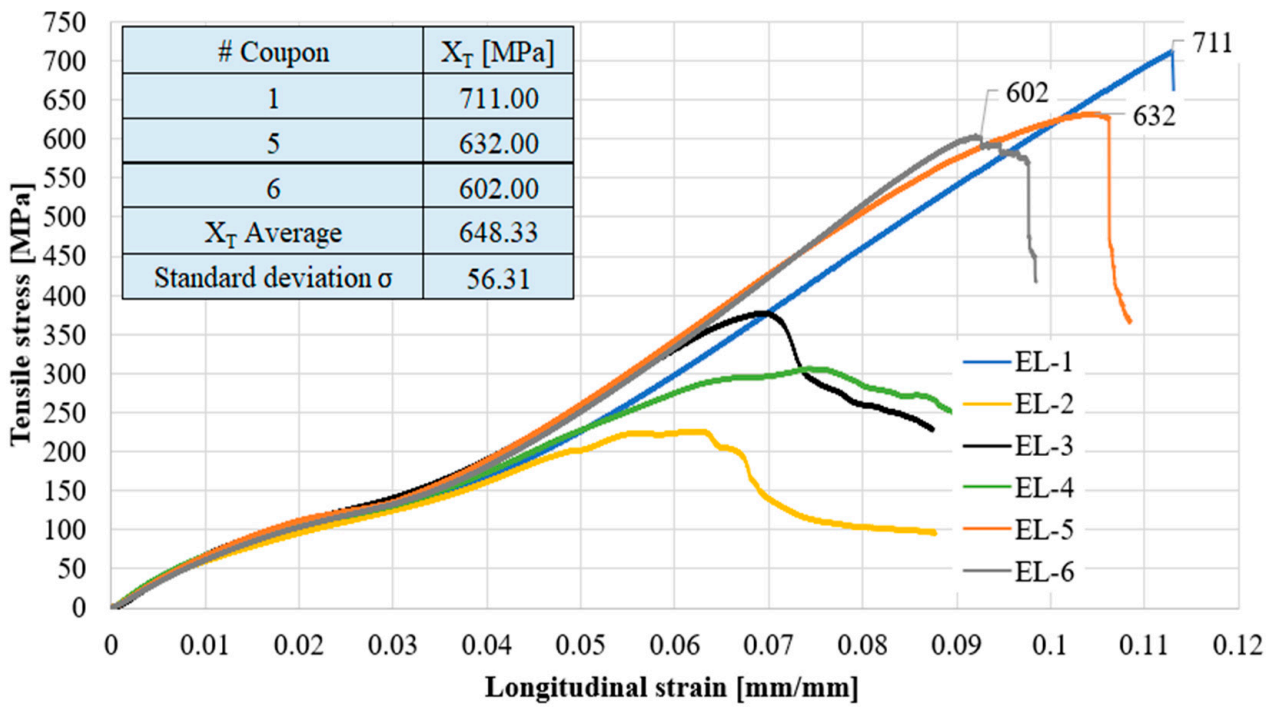


Figure 9. Tensile stress–strain curves of coupons tested at 0°. Coupons EL-5 and EL-6 were added. Strain measured with the universal machine.

Figure 10 shows the longitudinal strain–transversal strain curves of the coupons tested under tension at 0°, from which the Poisson’s ratio ($\nu_{LT} = 0.29 \pm 0.06$) was calculated.

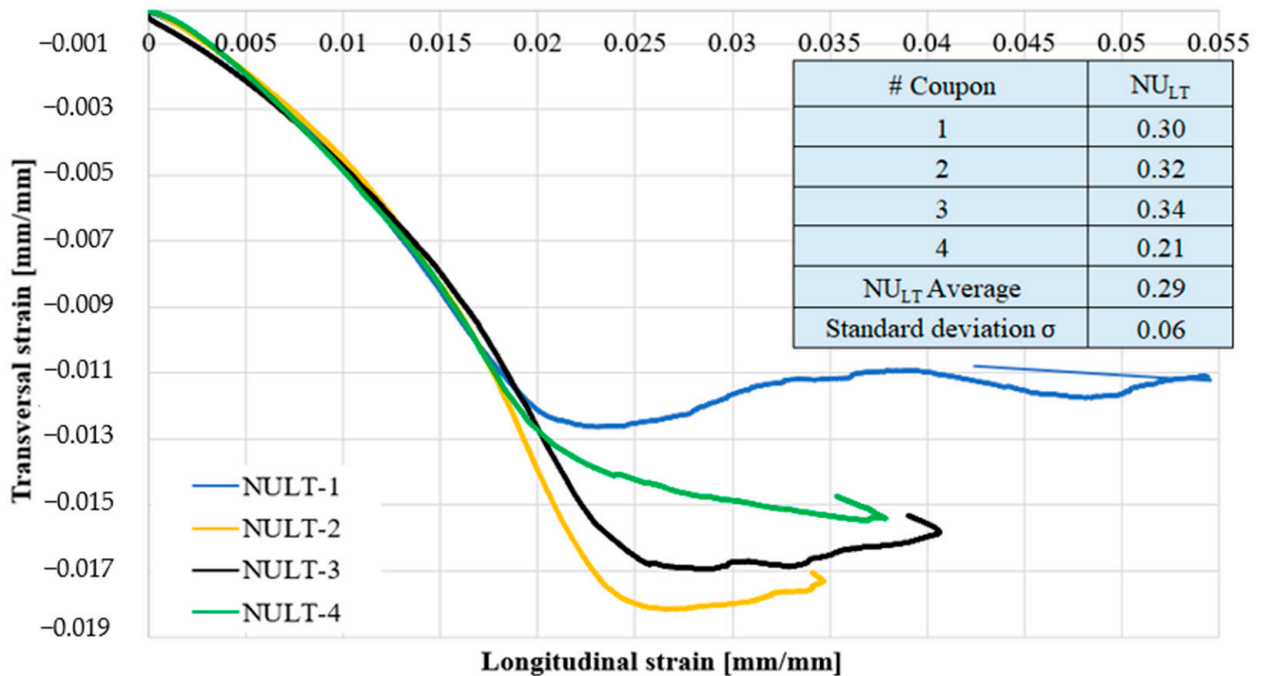


Figure 10. Poisson’s ratio ν_{LT} of coupons tested in tension at 0°. Strain measured with strain gages.

Figure 11 shows the coupons’ appearances after these tensile tests.



Figure 11. Condition of coupons after the tensile test at 0°.

Figure 12 shows the tensile stress–strain curves of four coupons tested at 90° (transversal direction). Due to the debonding of one of the tabs on coupon ET-3, it did not reach the strength and deformation of the other three coupons; however, the four coupons performed similarly in the 0–2% strain range, which was adequate to calculate the transversal elastic modulus ($E_T = 15.38 \pm 1.34$ GPa). The strength calculation ($Y_T = 659.57 \pm 20.42$ MPa) was made excluding coupon ET-3. Figure 13 shows the coupons' appearances after these tensile tests.

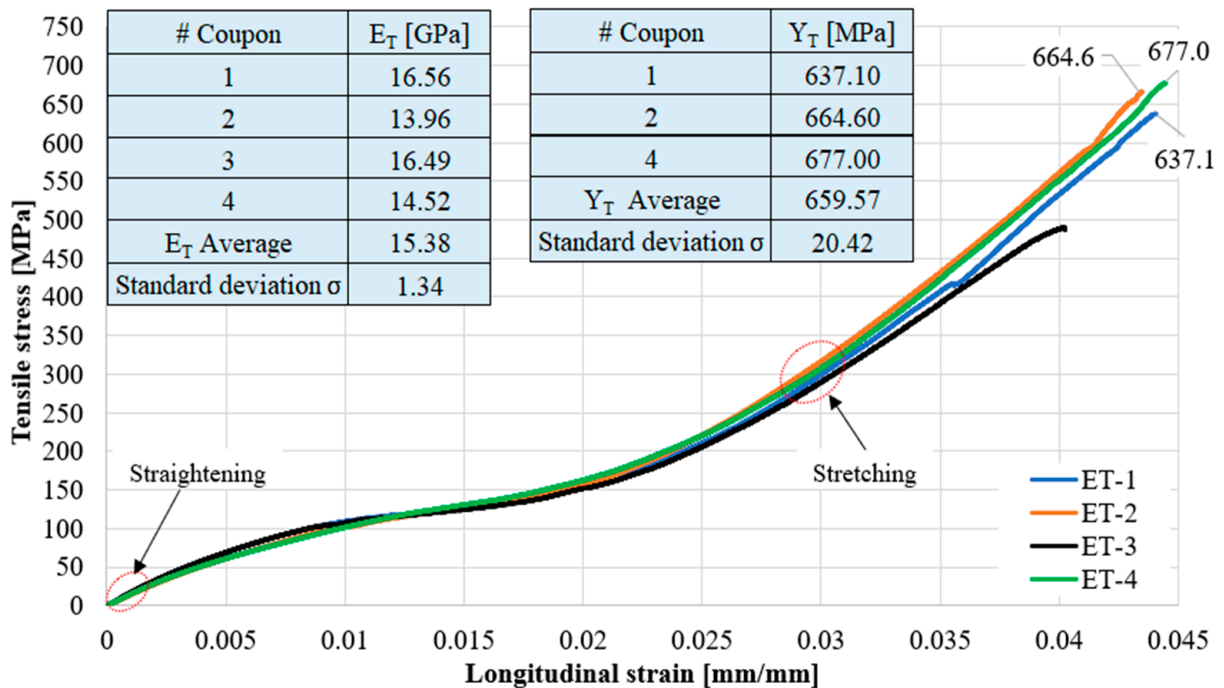


Figure 12. Tensile stress–strain curves of coupons tested at 90°. Strain measured with strain gages.



Figure 13. Condition of coupons after the tensile tests at 90° .

Experimental characterization of the stress–strain behavior of the coupons in the 0° and 90° directions revealed two distinct slopes (see Figures 8 and 12). The first slope corresponds to the straightening and the second to the stretching of the yarns until the rupture; this behavior was also noted by Gower et al. [15].

According to our study, the interwoven material is stiffer in the transversal direction than in the longitudinal direction because the former corresponds to the warp direction of the woven fabric; the orthotropic directions of the material were defined in Figure 2. This difference between E_L and E_T was reported by Ito, who attributed it to the tension control during the weaving manufacturing process [22]. Indeed, they observed that the yarns in the warp direction were almost straight, while in the weft direction the yarns weaved above and below the warp yarns, giving rise to a small slope or elastic modulus due to the straightening of the yarns.

Figure 14 shows the tensile stress–strain curve of coupons oriented at $[+45^\circ, -45^\circ]_s$. It was not possible to determine the shear strength of the material from these curves because the tabs of all coupons were debonded. Despite this, it was feasible to calculate the elastic modulus in this direction ($E_{\mp 45_S} = 2.82 \pm 0.21$ GPa), as shown in Figure 15. Figure 16 shows the coupons' appearances after these tensile tests. As can be seen, the end edges of the coupons remained straight because symmetry was used in the laminate, which avoided twisting the coupons (right side of Figure 6). A high longitudinal strain of about 38% (Figure 14) was calculated because the laminate with the material oriented at 45° had the lowest stiffness, as can be seen graphically in Figure 17. Once E_L , E_T , $E_{\mp 45_S}$ and ν_{LT} were obtained, it was possible to calculate the shear modulus through Equation (19), which gave a value of $G_{LT} = 0.717$ GPa. Tsai–Hill failure criterion was used in Equation (21) to determine the shear strength considering a minimum longitudinal strength of 80 MPa (Figure 14). The Tsai–Hill criterion compares the stresses on the orthotropy system with their corresponding strength direction. The stresses in the orthotropy direction are calculated with the theory

of classical laminate model applying loads in the global system (Figure 7). The minimum shear strength obtained was $S = 40$ MPa [21,23].

$$\left(\frac{\sigma_L}{X_T}\right)^2 - \frac{\sigma_L\sigma_T}{(X_T)^2} + \left(\frac{\sigma_T}{Y_T}\right)^2 + \left(\frac{\sigma_{LT}}{S}\right)^2 \geq 1 \tag{21}$$

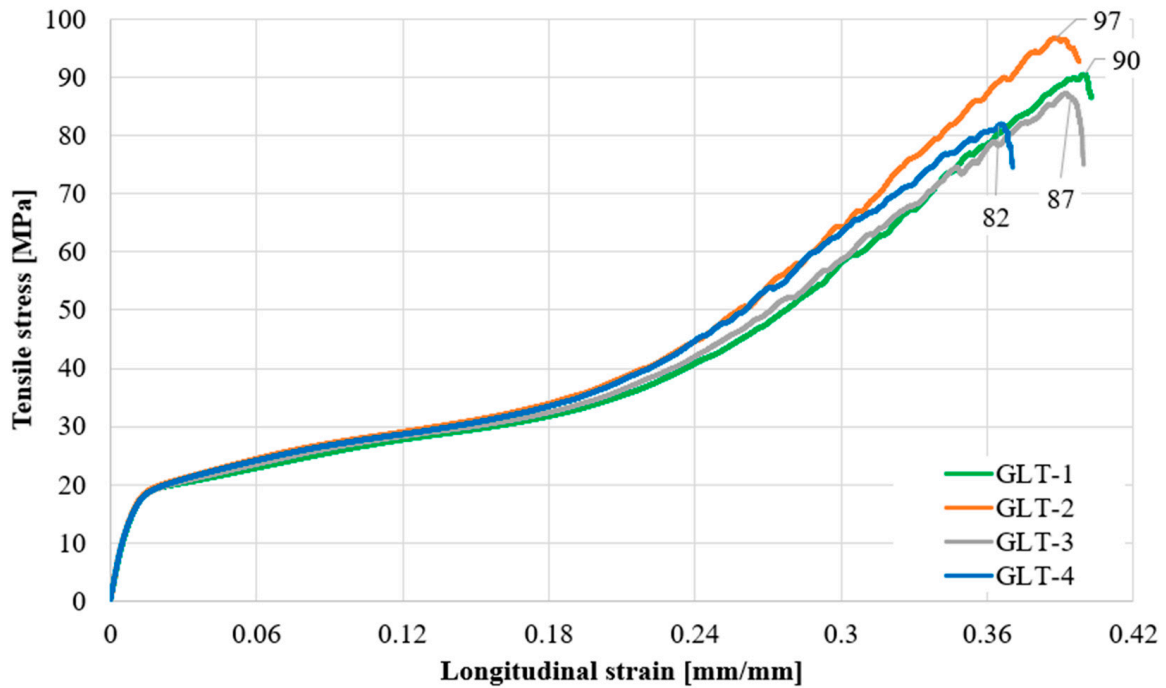


Figure 14. Tensile stress–strain curves of coupons tested at $[+45^\circ, -45^\circ]_s$. Strain measured with the universal machine.

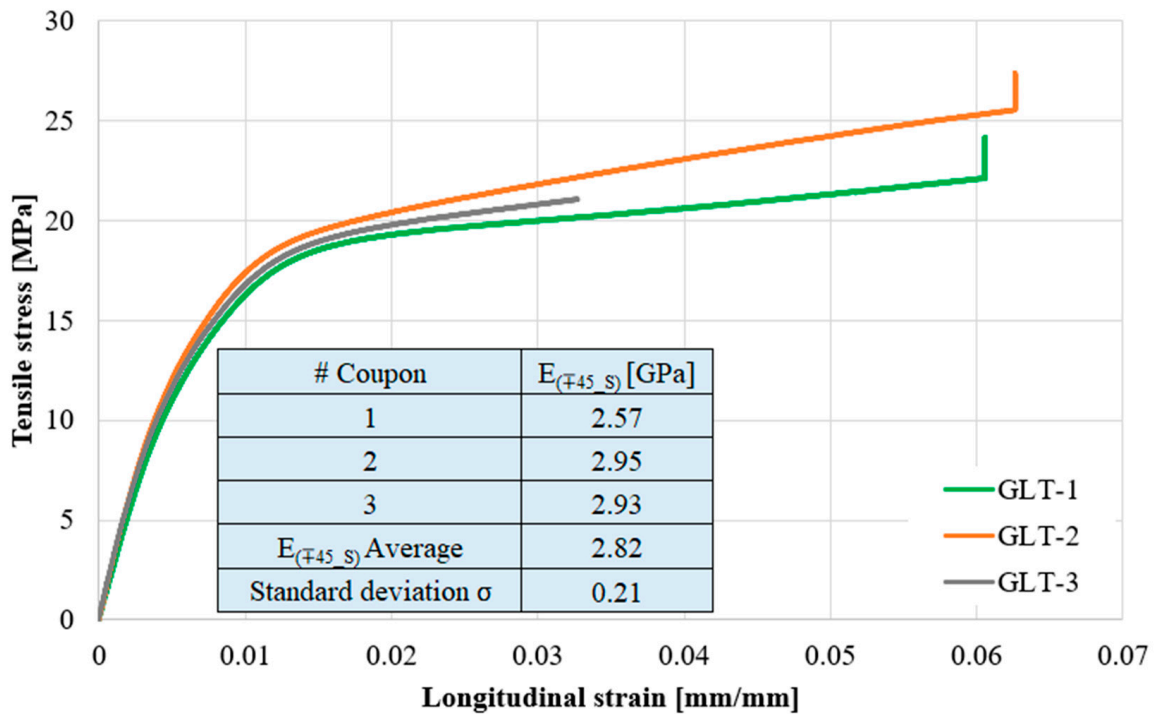


Figure 15. Tensile stress–strain curves of coupons tested at $[+45^\circ, -45^\circ]_s$. Strain measured with strain gages.

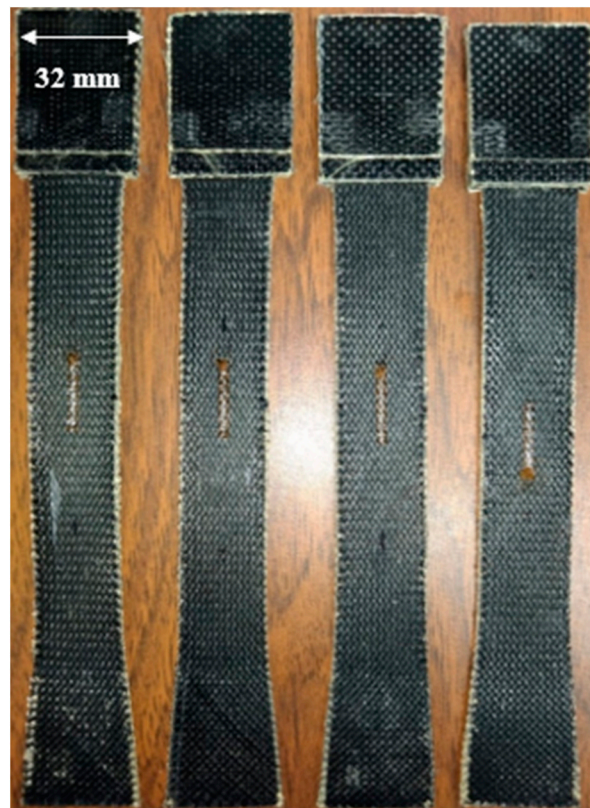


Figure 16. Condition of coupons after the tensile tests at $[+45^\circ, -45^\circ]_s$.

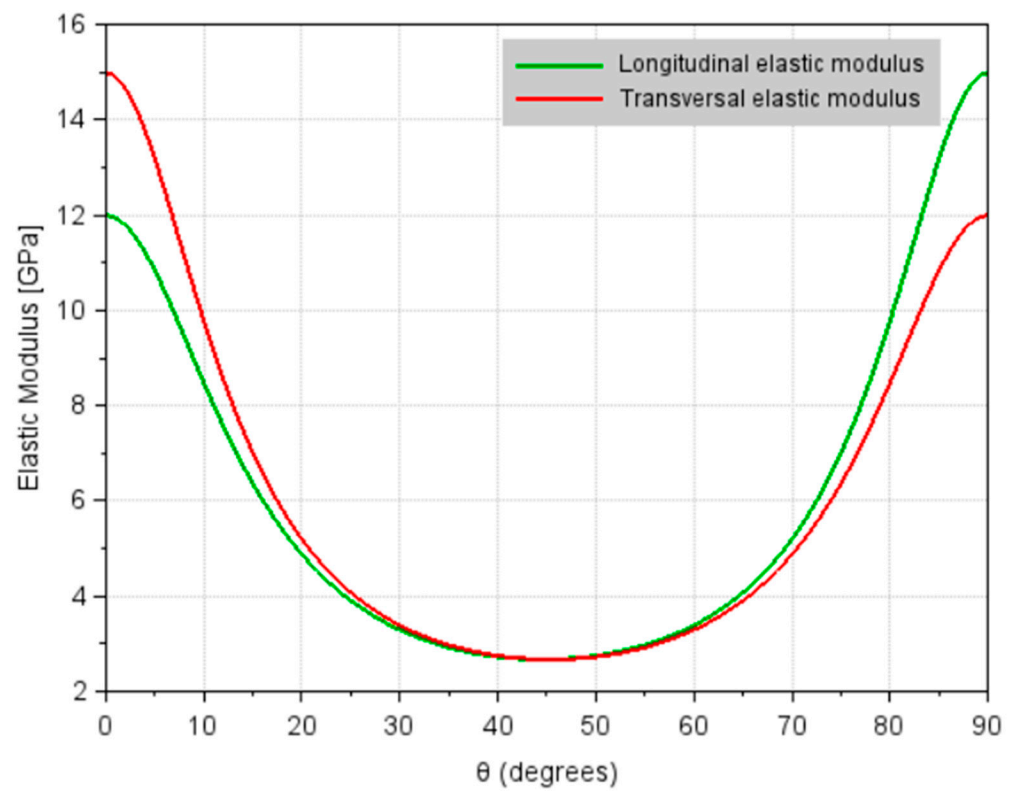


Figure 17. Evolution of the elastic moduli as a function of the laminate orientation.

Figure 18 presents a micrography of a damaged coupon far from the rupture region but close to the tab obtained with a VHX-7000 model Keyence® digital microscope. As can be seen, there is evidence of delamination.

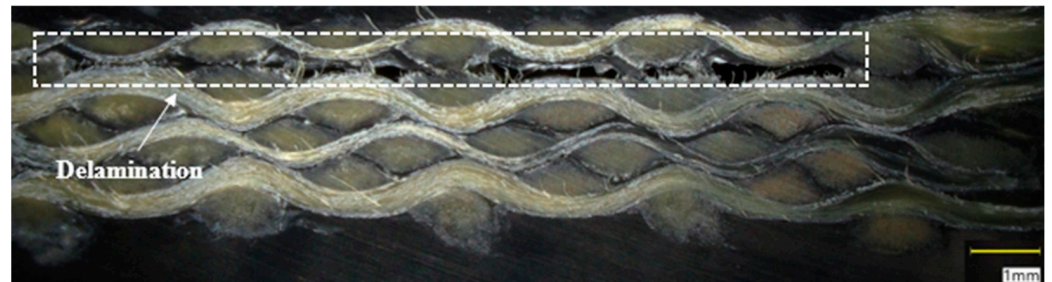


Figure 18. Micrography of a damaged coupon.

Table 2 summarizes the mechanical properties obtained in the present study, which are compared with other results found in the literature. As can be seen, the elastic moduli, shear modulus and strengths obtained in our work are of the same order of magnitude of those in the literature.

Table 2. Mechanical properties of Kevlar® composite obtained in this study compared with the literature.

Property	Present Work	van Hoof and Guoqi et al. [2,4]	Scazzosi et al. [14]	Nunes et al. [13]
Longitudinal elastic modulus, E_L [GPa]	11.78 (Weft direction)	18.50	10.06	7.618
Transversal elastic modulus, E_T [GPa]	15.38 (Warp direction)	18.50	10.06	11.05
Poisson's ratio, ν_{LT}	0.29	0.25	0.25	0.18
Shear modulus, G_{LT} [GPa]	0.717	0.77	0.77	2.123
Longitudinal Tensile strength, X_T [MPa]	648.33	555.00	425.00	400.00
Transversal Tensile strength, Y_T [MPa]	659.57	555.00	425.00	530.00
Shear strength, S [MPa]	>40.00	77.00	77.00	67.00

4. Conclusions

- A detailed methodology for the in-plane mechanical characterization of a Kevlar® composite based on quasi-static tensile tests was presented.
- An alternative to the Jones' method for the shear modulus calculation was proposed, which avoids moment generation in the grips and prevents the coupon from twisting.
- As observed in the results of the tests, debonding of the tabs of some coupons occurred; therefore, a time sweep study was performed at 192 °C using a TA® Instruments RSA3 DMA System (dynamic-mechanical analyzer) on a rectangular layer of 12 mm × 55 mm through a three-point bending test. The aim was to observe whether the 3 min of thermoforming given to the tabs was sufficient for them to adhere to the main body of coupons. Figure A1 in Appendix A shows the storage modulus (E'), showing that at a time of 328 s the stiffness remains stable. Therefore, at least 6 min of local thermoforming of the tabs must be applied to avoid their debonding during the tensile tests.

Author Contributions: Methodology: R.A.C.d.I.C. and A.D.D.; Resources: C.C.G. and L.A.Z.A.; Supervision: A.D.D., G.P.B. and J.M.H.R. All authors have read and agreed to the published version of the manuscript.

Funding: This research received no external funding.

Data Availability Statement: Data are contained within the article.

Acknowledgments: This work was published with the support of the Instituto de Innovación y Competitividad de la Secretaría de Innovación y Desarrollo Económico del Estado de Chihuahua. RACC thanks CONAHCYT for his scholarship (grant number 347734). Thanks are due to K. Campos Venegas, E. Ivonne Lopez Martínez, M.E. Mendoza Duarte, I.A. Estrada Moreno, J.E. Ledezma Sillas, R. Castañeda Balderas and D. Flores Hernandez for the shared expertise and technical support.

Conflicts of Interest: The authors declare no conflicts of interest.

Appendix A

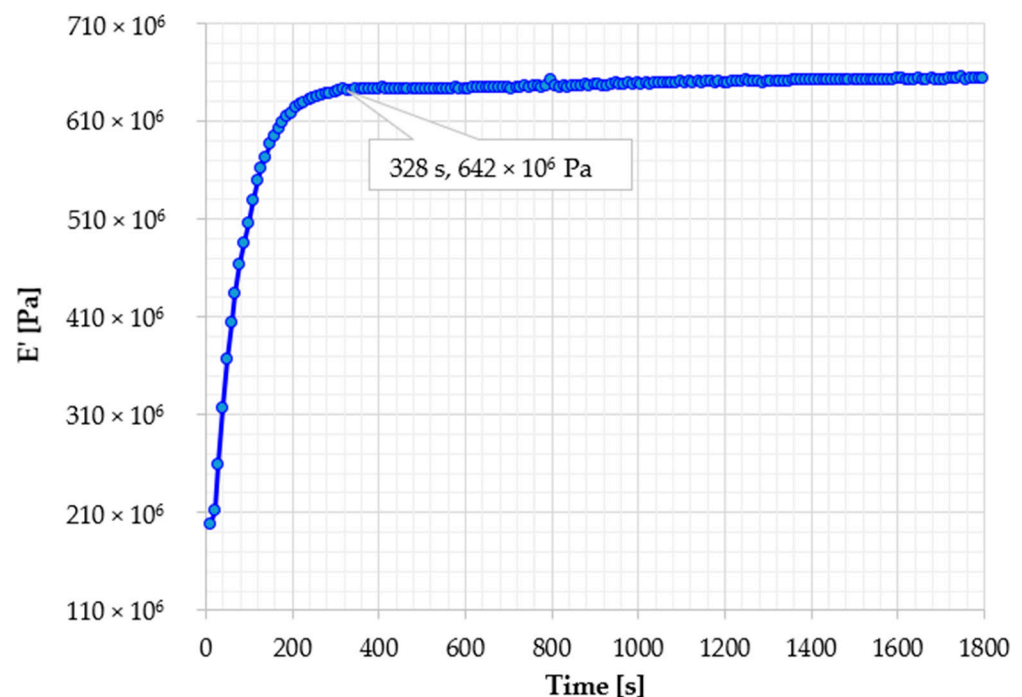


Figure A1. Time sweep obtained with a TA[®] Instruments RSA3 DMA System.

References

1. Bunsell, A.R.; Joannès, S.; Thionnet, A. *Fundamentals of Fibre Reinforced Composite Materials*; CRC Press: Boca Raton, FL, USA, 2021.
2. Hoof, J.V. Modelling of Impact Induced Delamination in Composite Materials. Ottawa-Carleton Institute for Mechanical and Aerospace Engineering. Doctoral Dissertation, Carleton University, Ottawa, ON, Canada, 1999.
3. Hoof, J.V.; Cronin, D.S.; Worswick, M.J.; Williams, K.; Nandlall, D. Numerical head and composite helmet models to predict blunt trauma. In Proceedings of the 19th International Symposium of Ballistics, Interlaken, Switzerland, 7–11 May 2001.
4. Guoqi, Z.; Goldsmith, W.; Dharan, C.H. Penetration of laminated Kevlar by projectiles—I. Experimental investigation. *Int. J. Solids Struct.* **1992**, *29*, 399–420. [[CrossRef](#)]
5. Moure-Guardiola, C.; Rubio, I.; Antona-Makoshi, J.; Olmedo, Á.; Loya, J.A.; Millán, M.R. Evaluation of Combat Helmet Behavior under Blunt Impact. *Appl. Sci.* **2020**, *10*, 8470. [[CrossRef](#)]
6. Lee, H.; Gong, S.W. Finite element analysis for the evaluation of protective functions of helmets against ballistic impact. *Comput. Methods Biomech. Biomed. Eng.* **2010**, *13*, 537–550. [[CrossRef](#)]
7. Palta, E.; Fang, H.; Weggel, D.C. Finite element analysis of the Advanced Combat Helmet under various ballistic impacts. *Int. J. Impact Eng.* **2018**, *112*, 125–143. [[CrossRef](#)]
8. Caçoilo, A.; Mourão, R.; Teixeira-Dias, F.; Azevedo, A.; Coghe, F.; Valente, R.A.F. Modelling ballistic impact on military helmets: The relevance of projectile plasticity. *Def. Technol.* **2021**, *17*, 1699–1711. [[CrossRef](#)]
9. Tan, L.B.; Tse, K.M.; Lee, H.P.; Tan, V.B.C.; Lim, S.P. Performance of an advanced combat helmet with different interior cushioning systems in ballistic impact: Experiments and finite element simulations. *Int. J. Impact Eng.* **2012**, *50*, 99–112. [[CrossRef](#)]

10. Palomar, M.; Lozano-Mínguez, E.; Rodríguez-Millán, M.; Miguélez, M.H.; Giner, E. Relevant factors in the design of composite ballistic helmets. *Compos. Struct.* **2018**, *201*, 49–61. [[CrossRef](#)]
11. Bresciani, L.M.; Manes, A.; Ruggiero, A.; Iannitti, G.; Giglio, M. Experimental tests and numerical modelling of ballistic impacts against Kevlar 29 plain-woven fabrics with an epoxy matrix: Macro-homogeneous and Meso-heterogeneous approaches. *Compos. Part B Eng.* **2016**, *88*, 114–130. [[CrossRef](#)]
12. Manes, A.; Bresciani, L.M.; Giglio, M. Ballistic Performance of Multi-layered Fabric Composite Plates Impacted by Different 7.62 mm Calibre Projectiles. *Procedia Eng.* **2014**, *88*, 208–215. [[CrossRef](#)]
13. Nunes, S.G.; Scazzosi, R.; Manes, A.; Amico, S.C.; de Amorim Júnior, W.F.; Giglio, M. Influence of projectile and thickness on the ballistic behavior of aramid composites: Experimental and numerical study. *Int. J. Impact Eng.* **2019**, *132*, 103307. [[CrossRef](#)]
14. Scazzosi, R.; Manes, A.; Petrone, G.; Giglio, M. Two different modelling approaches for fabric composites subjected to ballistic impact. *IOP Conf. Ser. Mater. Sci. Eng.* **2018**, *406*, 012051. [[CrossRef](#)]
15. Gower, H.L.; Cronin, D.S.; Plumtree, A. Ballistic impact response of laminated composite panels. *Int. J. Impact Eng.* **2008**, *35*, 1000–1008. [[CrossRef](#)]
16. Shim, V.P.W.; Lim, C.T.; Foo, K.J. Dynamic mechanical properties of fabric armour. *Int. J. Impact Eng.* **2001**, *25*, 1–15. [[CrossRef](#)]
17. Li, Y.Q.; Li, X.G.; Gao, X.-L. Modeling of Advanced Combat Helmet Under Ballistic Impact. *J. Appl. Mech.* **2015**, *82*, 111004. [[CrossRef](#)]
18. Tham, C.Y.; Tan, V.B.C.; Lee, H.P. Ballistic impact of a KEVLAR®helmet: Experiment and simulations. *Int. J. Impact Eng.* **2008**, *35*, 304–318. [[CrossRef](#)]
19. Daniel, I.M.; Ishai, O. *Engineering Mechanics of Composite Materials*; Oxford University Press: New York, NY, USA, 2006.
20. D3039/D3039M; Standard Test Method for Tensile Properties of Polymer Matrix Composite Materials. ASTM International: West Conshohocken, PA, USA, 2017.
21. Jones, R.M. *Mechanics of Composite Materials*; Taylor & Francis: Philadelphia, PA, USA, 1999.
22. Ito, M.; Chou, T.-W. An Analytical and Experimental Study of Strength and Failure Behavior of Plain Weave Composites. *J. Compos. Mater.* **1998**, *32*, 2–30. [[CrossRef](#)]
23. Diaz, A.; Castañeda, R.; Gameros, R.; Caron, J.-F.; Ehrlacher, A. MAC LAM: New Software for the Mechanical Analysis of Composites and Laminates. In Proceedings of the Seventh International Conference on Computational Structures Technology, Lisbon, Portugal, 7–9 September 2004.

Disclaimer/Publisher’s Note: The statements, opinions and data contained in all publications are solely those of the individual author(s) and contributor(s) and not of MDPI and/or the editor(s). MDPI and/or the editor(s) disclaim responsibility for any injury to people or property resulting from any ideas, methods, instructions or products referred to in the content.